JACS
JOURNAL OF THE AMERICAN CHEMICAL SOCIETY
Article
pubs.acs.org/JACS

Ultrathin Epitaxial Cu@Au Core–Shell Nanowires for Stable Transparent Conductors

Zhiqiang Niu,[†,‡,▽] Fan Cui,[†,‡,▽] Yi Yu,[†,§] Nigel Becknell,[†] Yuchun Sun,[†] Garo Khanarian,[∥] Dohyung Kim,[⊥] Letian Dou,[†,‡] Ahmad Dehestani,[‡] Kerstin Schierle-Arndt,[‡] and Peidong Yang*[,†,‡,⊥,#]

[†]Department of Chemistry, University of California, Berkeley, California 94720, United States
[‡]California Research Alliance (CARA), BASF Corporation, Berkeley, California 94720, United States
[§]Materials Sciences Division, Lawrence Berkeley National Laboratory, Berkeley, California 94720, United States
[∥]BASF Corporation, Union, New Jersey 07083, United States
[⊥]Department of Materials Science and Engineering, University of California, Berkeley, California 94720, United States
[#]Kavli Energy NanoSciences Institute at the University of California, Berkeley, and the Lawrence Berkeley National Laboratory, Berkeley, California 94720, United States

Supporting Information

ABSTRACT: Copper nanowire networks are considered a promising alternative to indium tin oxide as transparent conductors. The fast degradation of copper in ambient conditions, however, largely overshadows their practical applications. Here, we develop the synthesis of ultrathin Cu@Au core–shell nanowires using trioctylphosphine as a strong binding ligand to prevent galvanic replacement reactions. The epitaxial overgrowth of a gold shell with a few atomic layers on the surface of copper nanowires can greatly enhance their resistance to heat (80 °C), humidity (80%) and air for at least 700 h, while their optical and electrical performance remained similar to the original high-performance copper (e.g., sheet resistance 35 Ω sq^{-1} at transmittance of ∼89% with a haze factor <3%). The precise engineering of core–shell nanostructures demonstrated in this study offers huge potential to further explore the applications of copper nanowires in flexible and stretchable electronic and optoelectronic devices.

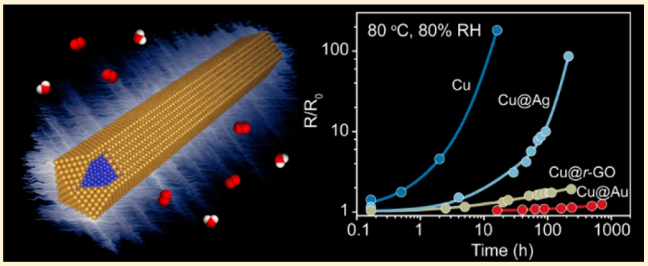

INTRODUCTION

Transparent conductors are an indispensable component in many optoelectric devices, such as touch panels, e-papers, photovoltaic devices, organic light emitting diodes, and electrochromic windows.[1,2] Although indium tin oxide (ITO) accounts for the great majority of the current market share,[3] the high cost of the sputtering process and low mechanical flexibility undermine its long-term dominance.[4] Tremendous efforts have been devoted to the development of the next-generation of transparent conductive materials. Among various options, metal nanowire networks are emerging as a promising alternative to ITO,[4−10] especially in flexible and stretchable electronics.[11,12] This is mainly because they have low processing cost, low sheet resistance, high optical quality, and excellent mechanical flexibility.

Copper is arguably one of the best metal materials for transparent conductors. Copper has the second best intrinsic conductivity among all elements with an electrical resistivity of 1.7×10^{-8} Ω·m, comparable to silver (1.6×10^{-8} Ω·m) and 30% better than gold (2.2×10^{-8} Ω·m).[13] Meanwhile, copper is much more abundant than silver by 1000 times or gold by 22 000 times.[14] High-transmittance copper nanowire thin films with low sheet resistances have been demonstrated.[15−22] For example, our group recently developed the synthesis of copper nanowires with diameters below 20 nm. These ultrathin nanowires are highlighted by their low haze factor of 2−3% with a transparency of 90% at a sheet resistance of 35 Ω sq^{-1}, making them among the highest-performing substitute for ITO.[16] However, copper is extremely vulnerable to species like O_2, H_2O, and sulfide in ambient atmosphere.[23] It suffers from rapid oxidation and consequent steep performance decline.[24] Considerable research has been devoted to solve this stability issue, mostly by exploiting a core–shell structure that encapsulates copper with an inert shell. A large spectrum of materials have been explored as the protective shell, such as graphene,[25,26] graphene oxide,[24] metal oxides,[27,28] and metals.[29−33] Graphene and graphene oxide have been demonstrated to enhance copper's resistance toward oxidation while keeping or even slightly promoting nanowires' electrical contacts. However, the protection is impaired under harsh environments due to the difficulty of achieving a complete and well-defined coverage.[24] The high conductivity of graphene can even promote the electrochemical reaction at the interface and

Received: March 22, 2017
Published: May 8, 2017

DOI: 10.1021/jacs.7b02884
J. Am. Chem. Soc. 2017, 139, 7348−7354

catalyze the corrosion of copper over long time scales.[34] Metal oxides usually result in outstanding protections, yet electrical conductivity is often scarified. Coating of metals generally provides a good solution with both oxidation protection and electrical contacts. In particular, a recent study by Stewart et al. coated Cu nanowires with Ag, Au and Pt shells.[33] The Cu@Ag nanowires with a shell thickness of ~5 nm exhibit comparable performance to pure silver or copper nanowires, while the protection of the copper core under humid conditions is not sufficient unless the shell thickness is increased to 15 nm. The enhanced stability endowed by the thick shell is at the expense of optical performance, especially the haze factor which is proportional to nanowire diameter.[35,36] Although the underlying reason for the insufficient protection using thin shells is largely unclear, the imperfect coverage of inert shell on copper surface and the indefinite interface between shell material and copper may play critical roles. We envision that this issue can be addressed through the epitaxial growth of a conformal and uniform shell of noble metal with a few atomic layers on copper nanowires.

The epitaxial overgrowth of a noble metal onto the surface of a less noble metal represents a synthetic challenge. Galvanic replacement usually dominates the growth process and results in hollow nanostructures.[37,38] Yang et al. revealed that galvanic reaction between Ag and $HAuCl_4$ could be blocked in the presence of strong reducing agents.[39] Another synthetic strategy demonstrated by Gao et al. suggested that the galvanic replacement-free overgrowth can be achieved by simultaneously decreasing the reduction potential of gold salts and providing sufficient protection on the metallic silver surface.[40] Herein, we show a successful case of epitaxial deposition of a conformal, ultrathin (1−2 nm) gold shell on the surface of copper nanowires by modifying the ligand environment of the gold precursor solution. Transparent conducting thin films made from the Cu@Au hold comparable optical and electrical properties to the parent ultrathin copper nanowires. More importantly, their high performance can be sustained under 80% humidity at 80 °C for a test duration of more than 700 h, the first demonstration of this level of long-term stability to the best of our knowledge.

RESULTS AND DISCUSSION

Our attempts to synthesize Cu@Au core−shell nanowires started by sequential reduction of the two metals in a fashion of seeded growth (Scheme 1, route 1). The ultrathin copper nanowires were first prepared in oleylamine (OAm) using tris(trimethylsilyl)silane as a reducing reagent, and served as seed for gold deposition. After the depletion of most of the copper precursor, $HAuCl_4$ dispersed in oleylamine was quickly injected into the growth solution. The products turned out to be a mixture of small nanoparticles and nanowires (Figure S1a). Energy dispersive spectroscopy (EDS) mapping (Figure S1b) shows that the small nanoparticles are pure gold, while the nanowires are composed of copper and gold, although the gold content is as low as 1% according to EDS quantitative analysis. There are some pits on the surface of nanowires, as revealed in the high-angle annular dark-field scanning transmission electron microscopy (HAADF-STEM) image (top left of Figure S1b). It implies the oxidation of the copper nanowires with $HAuCl_4$. The small nanoparticles could be separated via differential-speed centrifuging (Figure S1c). The characteristic localized-surface-plasmon-resonance (LSPR) observed at 525 nm in the ultraviolet−visible (UV−vis) spectrum (Figure S1d),[41] along

Scheme 1. Reduction of $HAuCl_4$ in the Presence of Cu Nanowire Seed under Different Ligand Environments and Injection Rates[a]

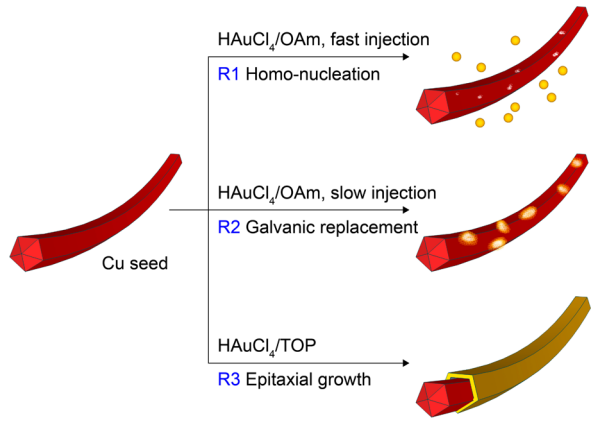

[a]With weakly bound ligand, such as oleylamine (OAm), fast injection induced homogeneous-nucleation of Au(0) species, while slow injection led to the domination of galvanic replacement between gold cations and Cu nanowires. With strongly bound ligand, such as trioctylphosphine (TOP), epitaxial growth was favored, independent of the injection rates.

with the powder X-ray diffraction (XRD) patterns (Figure S1e), further confirms the fact that they are gold nanoparticles. We rationalized this observation to be a consequence of homogeneous-nucleation at the initial stage of gold reduction. As $HAuCl_4$ was rapidly introduced into the growth solution, instantaneous reduction of the gold precursor led to a rapid increase of the concentration of gold atoms, initiating the nucleation and crystal growth on their own. We therefore modified the synthesis and slowly fed $HAuCl_4$ into the growth solution via syringe pump (Scheme 1, route 2). In this way, the concentration of newly formed gold atoms could be maintained at a relatively low level. The absence of small gold nanoparticles in the products (Figure S2) indicates the homogeneous-nucleation was indeed suppressed using slow injection. Hower, pores and voids are prevalent in the obtained nanowires (Figure S2), suggesting the galvanic replacement dominates the growth.

The occurrence of galvanic replacement is not unexpected due to the more noble nature of gold compared to copper. One possible solution is to reduce the reduction potential of Au^{3+} by lowering its activity on the basis of the Nernst equation (eq 1):[42]

$$E_{red} = E^{\oplus}_{red} + \frac{RT}{zF} \ln\left(\frac{a_{Au^{3+}}}{a_{Au}}\right) \quad (1)$$

where E stands for the electrode potential, R for the gas constant, T for the absolute temperature, z for the charge exchanged per particle during the course of the reduction, F for the Faraday's constant, and $a_{Au^{3+}}$ and a_{Au} for the activities of the oxidized Au^{3+} and reduced gold species. Given that the activity of pure substances in condensed phases is usually taken as unity ($a_{Au} = 1$), the reduction potential therefore depends solely on the activity of Au^{3+} at a given temperature. The activity of Au^{3+} can be tuned through the process of complexation with a ligand (L) with a Lewis base functional group (eq 2):

$$Au^{3+} + nL \overset{k}{\leftrightarrow} AuL_n^{3+} \quad (2)$$

DOI: 10.1021/jacs.7b02884
J. Am. Chem. Soc. 2017, 139, 7348−7354

A high stability constant of the complex (k) and a high concentration of the Lewis base (a_L) will effectively decrease the activity of Au^{3+} ($a_{Au^{3+}}$), and thus its reduction potential. The stability of metal complexes can be qualitatively predicted and explained by hard and soft acids and bases (HSAB) theory.[43] Specific to our synthesis, the gold cation acts as a soft Lewis acid, but the coexisting Lewis bases like chloride (Cl^-, from $HAuCl_4$) and OAm ($C_{18}H_{35}NH_2$) are both hard. We therefore reasoned that the introduction of a soft Lewis base such as phosphine would strongly bind to the gold cation and keep its activity and thus the reduction potential low.

Given this, we optimized our synthesis using trioctylphosphine (TOP), a common phosphine ligand in colloidal synthesis,[44] to replace OAm in dissolving the gold precursor (Scheme 1, route 3). It should be mentioned that the injection speed does not matter too much under this condition as revealed by reduction kinetics studies using UV−vis spectroscopy. When $HAuCl_4$ was dispersed in OAm, a strong LSPR band emerged within 3 min after a quick injection at 140 °C (Figure S3a), reflecting the instant reduction of $HAuCl_4$ to gold nanoparticles. As a sharp comparison, the absorption spectrum showed little change even 30 min after the one-shot injection of $HAuCl_4$/TOP at the same temperature (Figure S3b), and the reaction solution remained colorless. This suggests the reduction kinetics of Au^{3+} are quite sluggish in the presence of TOP. Since the concentration of newly reduced gold atoms always stays low due to the retarded reduction rate, it is not necessary to use the time-consuming slow-injection strategy. The UV−vis spectroscopic study indicates that TOP is capable of changing the reduction kinetics of the Au precursor, although it was initially intended to modify the reaction thermodynamics by way of reducing the reduction potential of Au^{3+}.

Figure 1a depicts the transmission electron microscopy (TEM) image of the products obtained from the optimized synthetic protocol. Nanowires are in high purity with an average diameter of 21 ± 4 nm. In the enlarged TEM image (Figure 1b), the nanowires can be observed intact without any surface pores or voids. We also noticed that Moiré patterns spread over these nanowires, which is an indicator of the superimposition of two different phases with different lattice constants.[45] The lengths of the nanowires are in the range of 10 to 20 μm as shown in the scanning electron microscope (SEM) image (Figure 1c). HAADF-STEM shows a brighter contrast on the edges of the nanowires (Figure 1d), suggesting a local enrichment of the heavier gold atoms. The core−shell structural feature is confirmed by EDS mapping (Figure 1e−g). Whereas copper (green color) is distributed in the central zone of the nanowires, gold (red color) is mainly located in the outer region. The gold shell thickness is measured to be about 2 nm in average. The compositional line profiles of copper and gold across three aligned nanowires present an alternating pattern (Figure S4), also suggesting the core−shell distribution of the two elements. The bulk composition of the core−shell nanowires is determined to be $Cu_{86}Au_{14}$ via quantitative analysis of the EDS spectra. The gold content in the products is slightly lower than the feeding ratio of the metal precursors (Cu:Au = 5:1). This could be attributed to the incomplete consumption of Au precursor due to its sluggish reduction rate in the presence of TOP. To demonstrate the global uniformity of the gold shell on copper, we selectively removed the copper phase in the core−shell nanowires by acetic acid corrosion. Figure S5 shows TEM

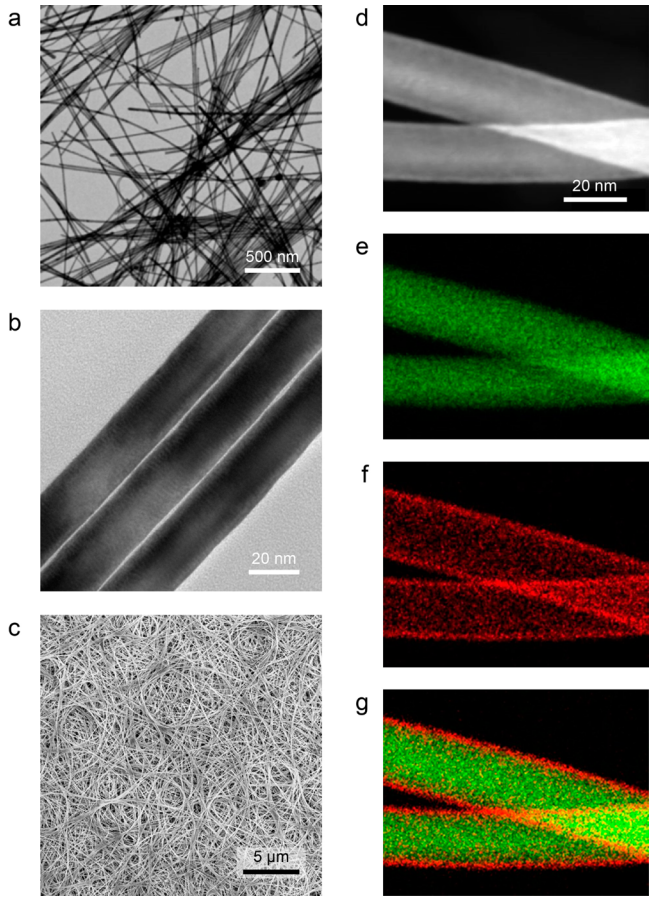

Figure 1. TEM images with different magnifications (a, b), SEM image (c), HAADF-STEM image (d), and the corresponding EDS mapping images (e−g) of Cu@Au core−shell nanowires. In the EDS maps, red color represents Au and green color represents Cu.

images of the corroded Cu@Au. High-quality nanotubes were generated after acid treatment. The uninterrupted shell of the nanotubes suggests the conformal, uniform, and complete coating of gold on the surface of copper nanowires. The successful preparation of Cu@Au core−shell nanowires demonstrates the aforementioned reasoning: the employment of soft Lewis base in the synthesis does redirect the growth pathway from galvanic replacement to surface deposition.

The thickness of the gold shell can be regulated with atomic precision by controlling the amount of gold precursor added into the reaction solution. As shown in Figure 2a−c, the shell thickness could be changed from ∼2 nm to ∼1.5 nm and ∼1 nm by altering the Cu:Au feeding ratio from 5:1 to 10:1 and 20:1, respectively. The core−shell nanowires are accordingly termed as Cu@Au (2 nm Au), Cu@Au (1.5 nm Au), and Cu@Au (1 nm Au). Atomic resolution HAADF-STEM images (Figure 2d−f) reveal the shells containing different numbers of gold atomic layers, approximately corresponding to 11, 7, and 4 layers, respectively. From the high-resolution STEM images, we also notice that the surface of the nanowires is quite smooth without the presence of cuprous oxide layers which are regularly observed in pure copper nanostructures. The uninterrupted lattice fringes from the core to the shell manifest the epitaxial growth of gold on copper. This is critical for the electrical properties and the stability of the nanowires because the number of interface defects are minimized in this manner. The distances between the adjacent lattice fringes in the cores

DOI: 10.1021/jacs.7b02884
J. Am. Chem. Soc. 2017, 139, 7348−7354

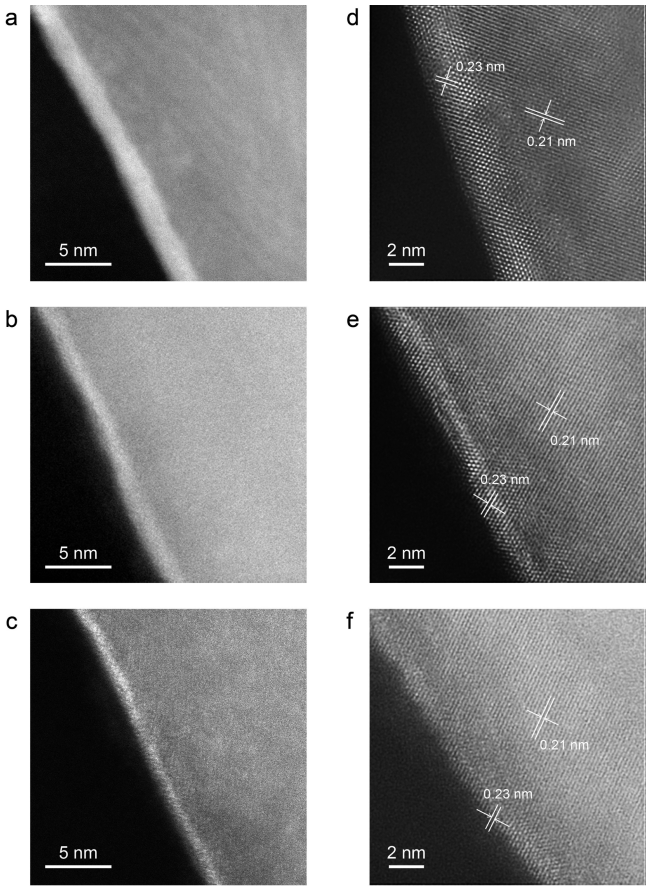

Figure 2. HAADF-STEM images of Cu@Au core–shell nanowires synthesized with Cu:Au feedings of 5:1 (a), 10:1 (b), 20:1 (c). Corresponding atomic resolution STEM images (d–f). Whereas the lattice distance in the core area is measured to be 0.21 nm, it is 0.23 nm in the shell area, agreeing well with the Cu(111) and Au(111) lattice spacings, respectively.

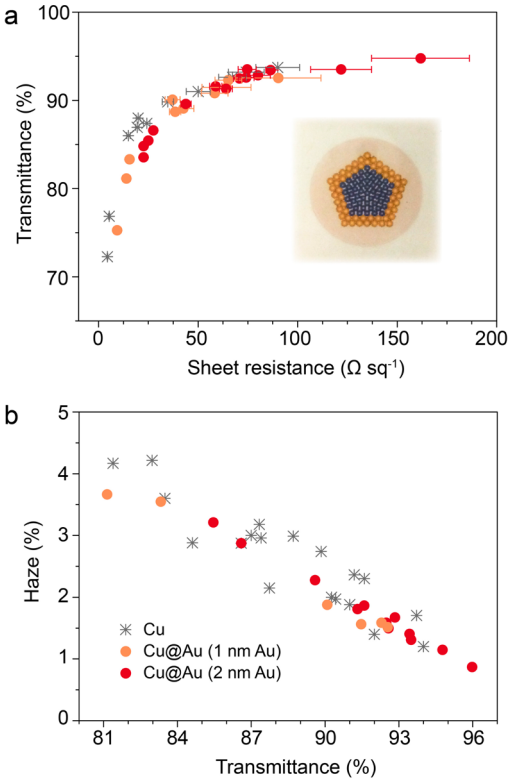

Figure 3. Plots of transmittance vs sheet resistance (a) and haze factor vs total transmittance (b) of transparent conductors made from bare copper nanowires, Cu@Au (1 nm Au) and Cu@Au (2 nm Au). Inset in (a) shows the optical image of Cu@Au (2 nm) nanowire film.

are measured to be 0.21 nm for all the three samples, in good agreement with the lattice spacing of the Cu(111) plane, while the distances in the shell areas expand to 0.23 nm.

Transparent conducting films were made on thin glass slides using vacuum filtration method. As shown in Figure S6, the nanowires are evenly distributed throughout the film with no obvious aggregation. The UV–vis transmittance spectra of the core–shell nanowire mesh made from Cu@Au (1 nm Au) and Cu@Au (2 nm Au) are given in Figure S7. Overall, the films are highly transparent in a large wavelength window, from 350 to 1700 nm. Both cases of the core–shell films have the copper signature plasmon absorption dip at around 550 nm.[16] However, a notable flattening of the copper feature was observed for the thicker shell conductors due to the increased content of gold.

Figure 3 summarizes the optical and electrical performance of the Cu@Au core–shell nanowire electrodes, which exhibit excellent figures of merit in transparency, conductivity and haze. Figure 3a plots the transmittance versus sheet resistance relationship of three types of nanowire mesh films: bare Cu, Cu@Au (1 nm Au) and Cu@Au (2 nm Au). Even though the electrical conductivity of bulk gold is 30% lower than that of copper, the Cu@Au core–shell nanowires exhibit almost identical transparency-resistivity performance to bare Cu nanowires. No obvious degradation of electrical conductivity was observed after gold overgrowth due to the ultrathin nature of the shell layer. However, we do see a slight decrease in the conductivity in denser films. This is because when more material is applied, the contribution of bulk metal's intrinsic conductivity cannot be ignored. The inset of Figure 3a is the optical image of the Cu@Au nanowire film. The background pattern is seen in excellent clarity. We also calculated the electrical and optical properties of the Cu@Au nanowires using the semiempirical models (see Supporting Information) developed previously for Ag[46] and Cu@*r*-GO core–shell[24] nanowires. The calculated transmittance versus sheet resistance is shown in Figure S8a. This simulation agrees well with experimental data. The decrease in conductivity is most likely introduced by the more resistive gold shell and its contact.

Another important figure of merit of transparent conductors is their light-scattering effect, which is quantified in haze factor. Figure 3b presents the haze factor of the three types of films as a function of their total transmittance. In general, the haze factors of all three conductors decrease linearly with total transmittance. The small values of haze factors of the core–shell nanowire electrodes indicate that the light-scattering is minimized by their ultrathin dimension. When the total transmittance is at 91.5% for the 2 nm gold shell nanowire mesh, the haze factor is only 1.85%; this value is even smaller for the 1 nm gold shell nanowire mesh, which is 1.56% at the same total transmittance. Interestingly, the core–shell nanowire network exhibits the same level of, or even slightly lower, haze values compared to the bare copper electrodes. This result is counterintuitive because larger haze factor is expected with the increase in the mean diameter.[46] The reduced haze and scattering could result from the differences in the optical

DOI: 10.1021/jacs.7b02884
J. Am. Chem. Soc. 2017, 139, 7348–7354

properties of the two metals, as suggested by finite-difference time-domain (FDTD) simulations.[47] Our semiempirical simulations show very close haze values between the Cu and the Cu@Au core−shell nanowires (Figure S8b), supporting that the ultrathin gold shells (≤2 nm) hardly sacrifice the optical properties of the parental Cu nanowires.

Finally, we tested the core−shell nanowire conductors' ability to sustain their original conductivity and showed that the electrodes exhibit spectacular resistance toward degradation. The standard harsh condition (80 °C, 80 ± 5% humidity in air atmosphere) was used to evaluate the nanowires' stability toward oxygen, moisture and heat. The results are shown in Figure 4a. Seven individual Cu@Au (2 nm Au) films with

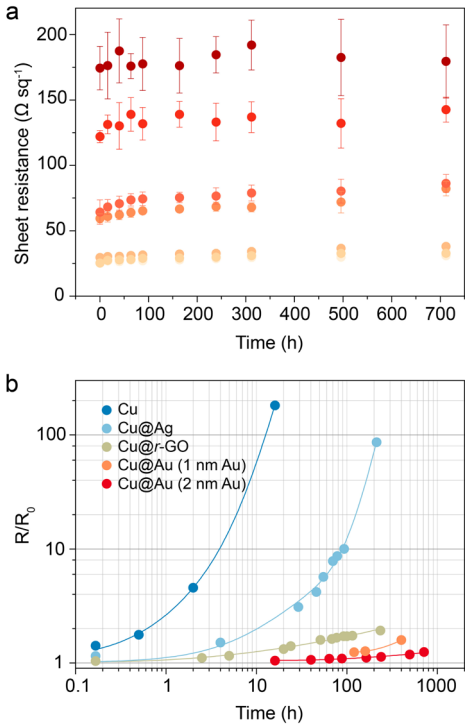

Figure 4. (a) Stability of Cu@Au (2 nm Au) core−shell nanowire mesh films in high humidity and high temperature environment (temperature = 80 °C, humidity = 80 ± 5%). Different colored labels represent films with different wire loading amounts. (b) Stability comparison of nanowire transparent electrodes made from bare Cu, Cu@Ag (with a composition of $Cu_{90}Ag_{10}$), Cu@*r*-GO, Cu@Au (1 nm Au), and Cu@Au (2 nm Au).

different wire loadings were placed under heated, high-humidity environment and their conductivity was traced with time. Impressively, throughout the 712 h of testing, the films maintained almost the same level of conductivity independent of the initial loading amount.

Figure 4b compares the harsh-environment aging behavior of the conducting films made from nanowires with different composition. Not surprisingly, the unprotected copper nanowire has the worst stability. After 1 h of exposure, the sheet resistance increased more than 4-fold. After 3 h, almost no conductivity could be measured in the copper nanowire mesh. Cu@Ag core−shell nanowires (Figure S9) appear to be more durable than bare copper, but still show considerable decay in conductivity. After 48 h of exposure to the harsh environment, the resistance increased almost 6 times. Our previously reported Cu@*r*-GO nanowire electrodes exhibit significant enhancement in stability.[24] After degradation treatment for 48 h, the sheet resistance only increased by 40%. The Cu@Au nanowires reported here are undoubtedly the most stable. After being exposed to high temperature and high humidity environment for 48 h, when most copper-based nanowire electrodes lose conductivity, gold-protected nanowires show no sign of degradation. The thicker the gold shell is, the more enduring the film can be. In the case of Cu@Au nanowire with 2 nm of Au shell, the sheet resistance increased by 24% throughout the 712 h of testing. The remarkable stability of Cu@Au core−shell nanowires can be mainly accredited to the epitaxial growth of gold shell. This synthesis provides a route to uniform and complete coverage of gold on the copper surface. Moreover, the epitaxial nucleation affords a thin, single-crystalline gold shell, which leaves few sites for oxygen or water to oxidize the interior copper atoms.

To investigate the aging mechanism of Au@Cu core−shell nanowires under harsh conditions, ambient pressure X-ray photoelectron spectroscopy (AP-XPS) experiments were performed at Beamline 9.3.2 of the Advanced Light Source by introducing 185 mTorr H_2O and 65 mTorr O_2 into the UHV chamber. The ratio was chosen to reflect a similar ratio of water to oxygen as is present in 80% humidity, the condition of the harsh stability test applied to these nanowires. The temperature of the sample was first raised to 80 °C, followed by heating to 100 and 120 °C. At each temperature, the sample was allowed to equilibrate until consecutive spectra looked identical. For Cu@Au (1 nm Au) nanowires, an increase in Cu:Au ratio at their surface was observed after increasing the temperature to 80 °C in the humidified oxygen atmosphere of the chamber (Figure 5a). Increasing the temperature to 100 or 120 °C brought about a slight further increase in the amount of copper at the surface of the Cu@Au (1 nm Au) sample. The increase in copper concentration at the surface of this sample is attributed to the more oxophilic nature of copper than gold. The thin layer of gold does not shield the copper atoms well enough from the O_2 and H_2O molecules, and the increased thermal energy allows for the highly mobile Cu atoms to diffuse to the nanowire surface. An identical experiment was performed on the Cu@Au (2 nm Au) nanowires (Figure 5b). Up to 120 °C in the H_2O/O_2 atmosphere, no increase in copper concentration at the nanowire surface was observed indicating the improved stability of the Cu@Au (2 nm Au) core−shell nanowire due to a slightly thicker gold shell protecting the copper from oxidizing molecules on the surface.

CONCLUSION

In summary, in order to achieve super durable Cu-based transparent conductors resistant to a harsh environment, ultrathin Cu@Au core−shell nanowires have been prepared through seeded overgrowth. The introduction of a phosphine ligand is believed to reduce both the reduction potential and the reduction rate of the gold precursor, shifting the growth mechanism into a galvanic-replacement-free pathway that is compatible with rapid injection. This versatile synthesis is capable of producing core−shell nanowires with tunable shell thickness to atomic precision, complete and conformal coverage, and nearly perfect interface rendered by the epitaxial growth of the single-crystalline gold shell. These features have produced enormous benefits to the optical and electrical properties as well as the stability of transparent conductive films. Compared to the original high-performance ultrathin Cu nanowires, transparent films fabricated from Cu@Au core−

DOI: 10.1021/jacs.7b02884
J. Am. Chem. Soc. 2017, 139, 7348−7354

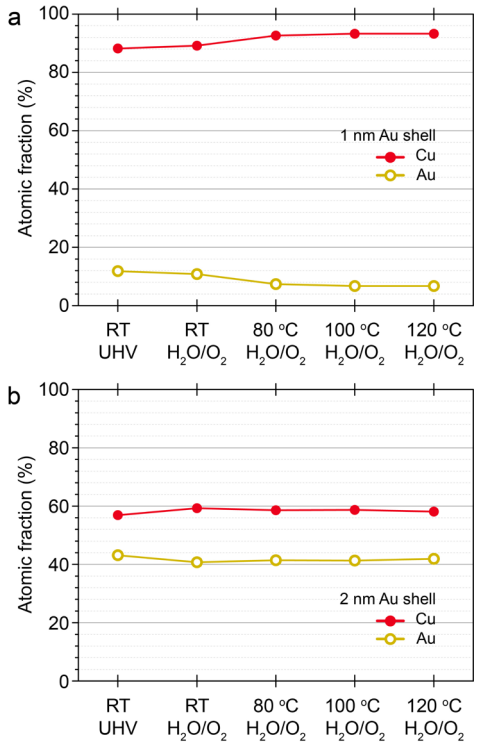

Figure 5. Variations of the surface atomic fractions of (a) Cu@Au (1 nm Au) and (b) Cu@Au (2 nm Au) in response to heating while exposed to humidity and oxygen obtained by AP-XPS. Note that the surface Cu concentration increases by ~5% for Cu@Au (1 nm Au) from RT to 120 °C while remaining constant for Cu@Au (2 nm Au).

shell nanowires show comparable figures of merit in transparency, conductivity and haze. Furthermore, these thin films exhibited unprecedented stability under long-term exposure to heat, humidity and air, far surpassing other Cu-based core–shell nanowires. Our results highlight the significance of precise structure control over the protective shell materials in promoting the applications of Cu nanowires in transparent conductors, particularly under harsh conditions.

EXPERIMENTAL SECTION

Materials. Tris(trimethylsilyl)silane (TTMSS, 97%), copper(II) chloride dihydrate ($CuCl_2 \cdot 2H_2O$, 99.999%), oleylamine (70%), trioctylphosphine (90%), gold(III) chloride trihydrate ($HAuCl_4 \cdot 3H_2O$, ≥49.0%) and nitrocellulose filter membranes (25 mm diameter, 220 nm pore size) were purchased from Sigma-Aldrich. Toluene (≥99.9%) was purchased from Fisher Scientific. All chemicals were used as received without further purification.

Characterization. Transmission electron microscopy (TEM) was performed with a Hitachi H-7650. High-angle annular dark-field scanning transmission electron microscopy (HAADF-STEM), energy dispersive spectroscopy (EDS) mapping, and quantitative EDS were carried out with an FEI TitanX 60–300. Aberration-corrected high-resolution scanning transmission electron microscopy (AC-HRSTEM) was performed on a double aberration-corrected TEAM 0.5 microscope at 300 kV using a high-angle annular detector resulting in "Z-contrast" images. Experimental AC-HR STEM images were deconvoluted using the maximum entropy method.[48] Scanning electron microscope (SEM) images were obtained on a JEOL JSM-6340F field emission scanning microscope. X-ray diffraction (XRD) was acquired using a Bruker D-8 General Area Detector Diffraction System (GADDS) with HI-STAR area charge-coupled device (CCD) detector, equipped with a Co Kα source (λ = 1.789 Å). Sheet resistance of nanowire thin films was measured using a CDE-RESMAP-270 four-point probe resistivity mapper. The transmittance and haze measurement was carried out on a Shimadzu UV-2550 UV–vis–NIR spectrophotometer with an integrating sphere. Ambient pressure X-ray photoelectron spectroscopy (AP-XPS) was performed at the Scienta R4000 HiPP endstation at the Lawrence Berkeley National Laboratory Advanced Light Source (ALS) Beamline 9.3.2. Samples were prepared on silicon substrates and mounted on a ceramic button heater sample holder in order to heat the sample up to 120 °C during experiments. The atmosphere was controlled at UHV (~10^{-9} Torr) or by introducing H_2O and O_2 gases into the chamber through different molecular leak valves. XPS spectra were collected using an incident X-ray energy of 390, 490, or 750 eV. The binding energy for XPS spectra was calibrated to the valence band spectra of the metallic nanowires. The XPS spectra were quantitatively analyzed by subtracting a Shirley background.

Synthesis of Cu@Au Nanowires. In a typical synthesis, $CuCl_2 \cdot 2H_2O$ (85 mg, 0.5 mmol) and oleylamine (0.5 g) were charged in a Schlenk flask. The mixture was stirred at 70 °C until the dissolution of the copper precursor. Tris(trimethylsily)silane (0.5 g, 2 mmol) was added into the solution under inert gas atmosphere. The resulting clear blue solution was slowly heated up from 70 to 120 °C in an oil bath. When the reaction solution turned into clear yellow at 120 °C, the reaction temperature was further raised to and kept at 165 °C for 18 h under stirring. Afterward, a TOP solution of $HAuCl_4 \cdot 3H_2O$ (0.1–0.025 M, 1 mL) was injected by syringe at 140 °C. The reddish reaction solution became crimson after the introduction of gold precursor, and was cooled down to room temperature 1 h later. The product was collected by centrifugation (6000 r.p.m., 5 min) and washed repeatedly with toluene using redispersion-centrifugation cycles to remove excess oleylamine. The product was dispersed in toluene for further characterization and film fabrication.

Fabrication of Transparent Conductive Film. To make a transparent conductive thin film, a dilute suspension of nanowires in toluene was made via sonication. The thin film was fabricated by filtering down the nanowire suspensions onto a nitrocellulose porous membrane (pore size 220 nm) under vacuum. The nanowire network was transferred to a transparent substrate (glass or PET) by applying pressure to the back side of the membrane and forcing an intimate contact with the substrate. The thin film was then annealed under forming gas (10% H_2 and 90% Ar) at 260 °C for 30 min to improve junction contact before measurements.

Transmittance and Haze Measurement. Background substrate transmittance has been subtracted from all the data. Characteristic transmittance and haze factors are acquired at 550 nm of wavelength. The haze measurement is carried out by D1003–13 standard. Four transmittance scans of a sample with different configurations were acquired for its haze calculations: T_1, incident light; T_2, total light transmitted by the specimen; T_3, light scattered by the instrument and T_4, light scattered by the instrument and specimen. The haze factor of 1 specimen can be calculated by the equation:

$$\text{Haze, \%} = [(T_4/T_2) - (T_3/T_1)]$$

Stability Test under Harsh Environment. Freshly made nanowire films were placed in air with temperature of 80 °C and water humidity of 80 ± 5%. The sheet resistance of films was tested with respect of time.

ASSOCIATED CONTENT

Supporting Information

The Supporting Information is available free of charge on the ACS Publications website at DOI: 10.1021/jacs.7b02884.

Details of optical simulations and additional figures (PDF)

AUTHOR INFORMATION

Corresponding Author

*p_yang@berkeley.edu

DOI: 10.1021/jacs.7b02884
J. Am. Chem. Soc. 2017, 139, 7348–7354

ORCID

Zhiqiang Niu: 0000-0002-9122-4880
Fan Cui: 0000-0003-3394-8095
Dohyung Kim: 0000-0003-0201-9082
Peidong Yang: 0000-0003-4799-1684

Author Contributions

[▽]ZN and FC contributed equally.

Notes

The authors declare no competing financial interest.

■ ACKNOWLEDGMENTS

This work was financially supported by BASF Corporation (Award Number 53093). Work at the NCEM, the Molecular Foundry and the Advanced Light Source was supported by the Director, Office of Science, Office of Basic Energy Sciences, of the U.S. Department of Energy under Contract No. DE-AC02-05CH11231. We acknowledge Ethan J. Crumlin and the use of Beamline 9.3.2 at the Advanced Light Source for collection of AP-XPS data. We acknowledge Chenlu Xie, Qiao Kong, and Hao Zhang for assistance with AP-XPS. D. K. acknowledges support from Samsung Scholarship.

■ REFERENCES

(1) Hosono, H.; Paine, D. C.; Ginley, D. S., Eds. *Handbook of Transparent Conductors*; Springer: New York, 2010.
(2) Gordon, R. G. *MRS Bull.* **2000**, *25*, 52.
(3) Ghaffarzadeh, K.; Das, R. *Transparent Conductive Films (TCF) 2016–2026*; Forecasts, Markets, Technologies (IDTechEx), 2016.
(4) Ye, S. R.; Rathmell, A. R.; Chen, Z. F.; Stewart, I. E.; Wiley, B. J. *Adv. Mater.* **2014**, *26*, 6670.
(5) Langley, D.; Giusti, G.; Mayousse, C.; Celle, C.; Bellet, D.; Simonato, J. P. *Nanotechnology* **2013**, *24*, 452001.
(6) De, S.; Higgins, T. M.; Lyons, P. E.; Doherty, E. M.; Nirmalraj, P. N.; Blau, W. J.; Boland, J. J.; Coleman, J. N. *ACS Nano* **2009**, *3*, 1767.
(7) Deng, B.; Hsu, P. C.; Chen, G. C.; Chandrashekar, B. N.; Liao, L.; Ayitimuda, Z.; Wu, J. X.; Guo, Y. F.; Lin, L.; Zhou, Y.; Aisijiang, M.; Xie, Q.; Cui, Y.; Liu, Z. F.; Peng, H. L. *Nano Lett.* **2015**, *15*, 4206.
(8) Guo, C. F.; Ren, Z. F. *Mater. Today* **2015**, *18*, 143.
(9) Lee, J. Y.; Connor, S. T.; Cui, Y.; Peumans, P. *Nano Lett.* **2008**, *8*, 689.
(10) Sun, Y. G.; Gates, B.; Mayers, B.; Xia, Y. N. *Nano Lett.* **2002**, *2*, 165.
(11) Lee, H.; Kim, I.; Kim, M.; Lee, H. *Nanoscale* **2016**, *8*, 1789.
(12) Sannicolo, T.; Lagrange, M.; Cabos, A.; Celle, C.; Simonato, J. P.; Bellet, D. *Small* **2016**, *12*, 6052.
(13) Giancoli, D. C. *Physics: Principles with Applications*; Prentice Hall: London, 1995.
(14) Ruben, S. *Handbook of the Elements*; Open Court: La Salle, 1985.
(15) An, S.; Jo, H. S.; Kim, D. Y.; Lee, H. J.; Ju, B. K.; Al-Deyab, S. S.; Ahn, J. H.; Qin, Y.; Swihart, M. T.; Yarin, A. L.; Yoon, S. S. *Adv. Mater.* **2016**, *28*, 7149.
(16) Cui, F.; Yu, Y.; Dou, L. T.; Sun, J. W.; Yang, Q.; Schildknecht, C.; Schierle-Arndt, K.; Yang, P. D. *Nano Lett.* **2015**, *15*, 7610.
(17) Guo, H. Z.; Lin, N.; Chen, Y. Z.; Wang, Z. W.; Xie, Q. S.; Zheng, T. C.; Gao, N.; Li, S. P.; Kang, J. Y.; Cai, D. J.; Peng, D. L. *Sci. Rep.* **2013**, *3*, 2323.
(18) Hsu, P. C.; Kong, D. S.; Wang, S.; Wang, H. T.; Welch, A. J.; Wu, H.; Cui, Y. *J. Am. Chem. Soc.* **2014**, *136*, 10593.
(19) Ye, S. R.; Rathmell, A. R.; Stewart, I. E.; Ha, Y. C.; Wilson, A. R.; Chen, Z. F.; Wiley, B. J. *Chem. Commun.* **2014**, *50*, 2562.
(20) Yin, Z.; Song, S. K.; You, D. J.; Ko, Y.; Cho, S.; Yoo, J.; Park, S. Y.; Piao, Y.; Chang, S. T.; Kim, Y. S. *Small* **2015**, *11*, 4576.
(21) Zhang, D. Q.; Wang, R. R.; Wen, M. C.; Weng, D.; Cui, X.; Sun, J.; Li, H. X.; Lu, Y. F. *J. Am. Chem. Soc.* **2012**, *134*, 14283.
(22) Zhong, Z.; Lee, H.; Kang, D.; Kwon, S.; Choi, Y. M.; Kim, I.; Kim, K. Y.; Lee, Y.; Woo, K.; Moon, J. *ACS Nano* **2016**, *10*, 7847.
(23) Scott, D. A. *Copper and Bronze in Art: Corrosion, Colorants, Conservation*; The Getty Conservation Institute: Los Angeles, 2002.
(24) Dou, L. T.; Cui, F.; Yu, Y.; Khanarian, G.; Eaton, S. W.; Yang, Q.; Resasco, J.; Schildknecht, C.; Schierle-Arndt, K.; Yang, P. D. *ACS Nano* **2016**, *10*, 2600.
(25) Xu, H. M.; Wang, H. C.; Wu, C. P.; Lin, N.; Soomro, A. M.; Guo, H. Z.; Liu, C.; Yang, X. D.; Wu, Y. P.; Cai, D. J.; Kang, J. Y. *Nanoscale* **2015**, *7*, 10613.
(26) Ahn, Y.; Jeong, Y.; Lee, D.; Lee, Y. *ACS Nano* **2015**, *9*, 3125.
(27) Chen, Z. F.; Ye, S. R.; Stewart, I. E.; Wiley, B. J. *ACS Nano* **2014**, *8*, 9673.
(28) Hsu, P. C.; Wu, H.; Carney, T. J.; McDowell, M. T.; Yang, Y.; Garnett, E. C.; Li, M.; Hu, L. B.; Cui, Y. *ACS Nano* **2012**, *6*, 5150.
(29) Lee, C.; Kim, N. R.; Koo, J.; Lee, Y. J.; Lee, H. M. *Nanotechnology* **2015**, *26*, 455601.
(30) Song, J. Z.; Li, J. H.; Xu, J. Y.; Zeng, H. B. *Nano Lett.* **2014**, *14*, 6298.
(31) Rathmell, A. R.; Nguyen, M.; Chi, M. F.; Wiley, B. J. *Nano Lett.* **2012**, *12*, 3193.
(32) Xue, J.; Song, J. Z.; Zou, Y. S.; Huo, C. X.; Dong, Y. H.; Xu, L. M.; Li, J. H.; Zeng, H. B. *RSC Adv.* **2016**, *6*, 91394.
(33) Stewart, I. E.; Ye, S. R.; Chen, Z. F.; Flowers, P. F.; Wiley, B. J. *Chem. Mater.* **2015**, *27*, 7788.
(34) Schriver, M.; Regan, W.; Gannett, W. J.; Zaniewski, A. M.; Crommie, M. F.; Zettl, A. *ACS Nano* **2013**, *7*, 5763.
(35) Hwang, J.; Lee, H.; Woo, Y. *J. Appl. Phys.* **2016**, *120*, 174903.
(36) Preston, C.; Xu, Y. L.; Han, X. G.; Munday, J. N.; Hu, L. B. *Nano Res.* **2013**, *6*, 461.
(37) Sun, Y. G.; Xia, Y. N. *Nano Lett.* **2003**, *3*, 1569.
(38) Fan, Z.; Luo, Z.; Huang, X.; Li, B.; Chen, Y.; Wang, J.; Hu, Y.; Zhang, H. *J. Am. Chem. Soc.* **2016**, *138*, 1414.
(39) Yang, Y.; Liu, J. Y.; Fu, Z. W.; Qin, D. *J. Am. Chem. Soc.* **2014**, *136*, 8153.
(40) Gao, C. B.; Lu, Z. D.; Liu, Y.; Zhang, Q.; Chi, M. F.; Cheng, Q.; Yin, Y. D. *Angew. Chem., Int. Ed.* **2012**, *51*, 5629.
(41) Ghosh, S. K.; Pal, T. *Chem. Rev.* **2007**, *107*, 4797.
(42) Bard, A. J.; Faulkner, L. R.; Leddy, J.; Zoski, C. G. *Electrochemical Methods: Fundamentals and Applications*; John Wiley & Sons: New York, 1980.
(43) Ho, T.-L. *Hard and Soft Acids and Bases Principle in Organic Chemistry*; Academic Press: New York, 1977.
(44) Niu, Z. Q.; Li, Y. D. *Chem. Mater.* **2014**, *26*, 72.
(45) Niu, Z. Q.; Becknell, N.; Yu, Y.; Kim, D.; Chen, C.; Kornienko, N.; Somorjai, G. A.; Yang, P. D. *Nat. Mater.* **2016**, *15*, 1188.
(46) Khanarian, G.; Joo, J.; Liu, X. Q.; Eastman, P.; Werner, D.; O'Connell, K.; Trefonas, P. *J. Appl. Phys.* **2013**, *114*, 024302.
(47) Kim, T.; Canlier, A.; Cho, C.; Rozyyev, V.; Lee, J. Y.; Han, S. M. *ACS Appl. Mater. Interfaces* **2014**, *6*, 13527.
(48) Grillo, V.; Rotunno, E. *Ultramicroscopy* **2013**, *125*, 97.

DOI: 10.1021/jacs.7b02884
J. Am. Chem. Soc. 2017, 139, 7348–7354